Direct ab Initio Dynamics Calculation of the Reaction Rates of CH_3OCl with OH

Hong-qing He, Jing-yao Liu, Ze-sheng Li,* and Chia-chung Sun

Institute of Theoretical Chemistry, State Key Laboratory of Theoretical and Computational Chemistry, Jilin University, Changchun 130023, People's Republic of China

Received: October 28, 2004; In Final Form: February 18, 2005

A direct ab initio dynamics method was carried out for the reaction $CH_3OCl + OH \rightarrow$ products. Three abstraction channels from chlorine atom, in-plane hydrogen, and out-of-plane hydrogen atoms at the CH_3 group have been found. The optimized geometries and frequencies of the stationary points and the minimum-energy paths (MEPs) were calculated at the MP2/6-311G(d,p) level. To improve the reaction enthalpy and potential barrier, single-point calculations were made at three higher levels of theory, the approximate QCISD(T)/6-311++G(3df,2pd), G3, and G3(MP2) levels. Furthermore, the rate constants for three abstraction channels were evaluated using canonical variational transition state theory (CVT) with the small-curvature tunneling correction (SCT) over a wide temperature range of 220−2000 K at above three higher theory levels, respectively. The calculated rate constants as well as branching rates are in reasonable agreement with the experimental values in the temperature region 250−341 K. The present results indicate H-abstraction especially from out-of-plane hydrogen is the main reaction pathway, while Cl-abstraction is much less competitive.

Introduction

Methyl hypochlorite (CH_3OCl) has been known to be an important atmospheric species since scientists found the severe depletions in stratospheric ozone during the Antarctic spring in 1985.[1,2] It is formed as a product in the reaction of methylperoxy radicals with ClO,[3,4] which is a prevalent and an important species in the chemistry of the atmosphere and in combustion systems where chlorine is present. Photolytic dissociation has been considered as a main possible route of release of chlorine from CH_3OCl. In addition, CH_3OCl is also expected to undergo homogeneous gas-phase photochemical reactions with Cl atoms and OH radicals. The rate constants of the two reactions are important to estimate whether CH_3OCl may take part in catalytic O_3 destroying cycles, or it may act as a relatively stable sink for chlorine leading to lower O_3 depletion rates. The aim of the present work is to study the reaction of CH_3OCl with OH.

The dynamic study has been performed on the reaction of CH_3OCl with OH.[5] For the reaction, H- and Cl-abstractions, are feasible.

$$CH_3OCl + OH \rightarrow CH_3O + HOCl \qquad (R1)$$

$$\rightarrow CH_2OCl + H_2O \qquad (R2)$$

With respect to H-abstraction channel R2, hydrogen atoms can be abstracted from in-plane and out-of-plane atoms, respectively, and, as a result, three transition states are located.

The experimental rate constants of $CH_3OCl + OH$ were reported by Crowley et al.,[5] and the Arrhenius expression was given by $k = (2.4 \pm 0.8) \times 10^{-12} \exp(-(360\pm100)/T)$ cm^3 molecule^{-1} s^{-1} in the temperature range 250−341 K. The results from Crowley et al. state that the title reaction leads to the formation of the products CH_2OCl and H_2O with 100% branching ratio. On the other hand, Kukui et al.[6] investigated the reaction of CH_3OCl with OH and considered that Cl-abstraction by OH would be the dominant reaction channel. In view of a different mechanism proposed by experiments, theoretical studies for the reaction $CH_3OCl + OH$ are very desirable.

Here, a dual-level direct dynamic approach (X//Y)[7−9] proposed by Truhlar and co-workers is employed to study the kinetic nature of the reaction $CH_3OCl + OH$. The information on the potential energy surface (PES) is obtained directly from ab initio electronic structure calculations. The rate constants for each reaction channel are calculated over a wide temperature range 220−2000 K using the variational transition state theory (VTST)[10−12] proposed by Truhlar and co-workers. Furthermore, the total rate constants and the product branching ratios are obtained.

Calculation Methods

All of the electronic structure calculations were carried out with the Gaussian 98 program[13] in our present study. The optimized geometries and harmonic vibrational frequencies of all of the stationary points (reactants, complexes, transition states, and products) are calculated at the restricted or unrestricted second-order Moller-Pleset perturbation theory with the 6-311G(d,p) basis set (MP2/6-311G(d,p)). The minimum energy path (MEP) is calculated by the intrinsic reaction coordinate (IRC) theory at the same level. The energy derivatives including gradients and Hessians at geometries along the MEP are obtained to calculate the curvature of the reaction path and to calculate the generalized vibrational frequencies along the reaction path at the same level. Because the shape of the MEP is important for the calculation of rate constants, single-point calculations are performed at the approximate QCISD(T)/6-311++G(3df,2pd) (denote as a-QCISD(T)),[14] G3,[15] and G3(MP2)[16] levels using the MP2/6-311G(d,p) optimized geometries. The dual-level potential profile along the reaction path is further refined with the interpolated single-point energies (ISPE) method,[17] in which a few extra single-point calculations are needed to correct the lower level reaction path.

* Corresponding author. Fax: +86-431-8498026. E-mail: ljy121@mail.jlu.edu.cn.

10.1021/jp045065t CCC: $30.25
Published on Web 03/19/2005

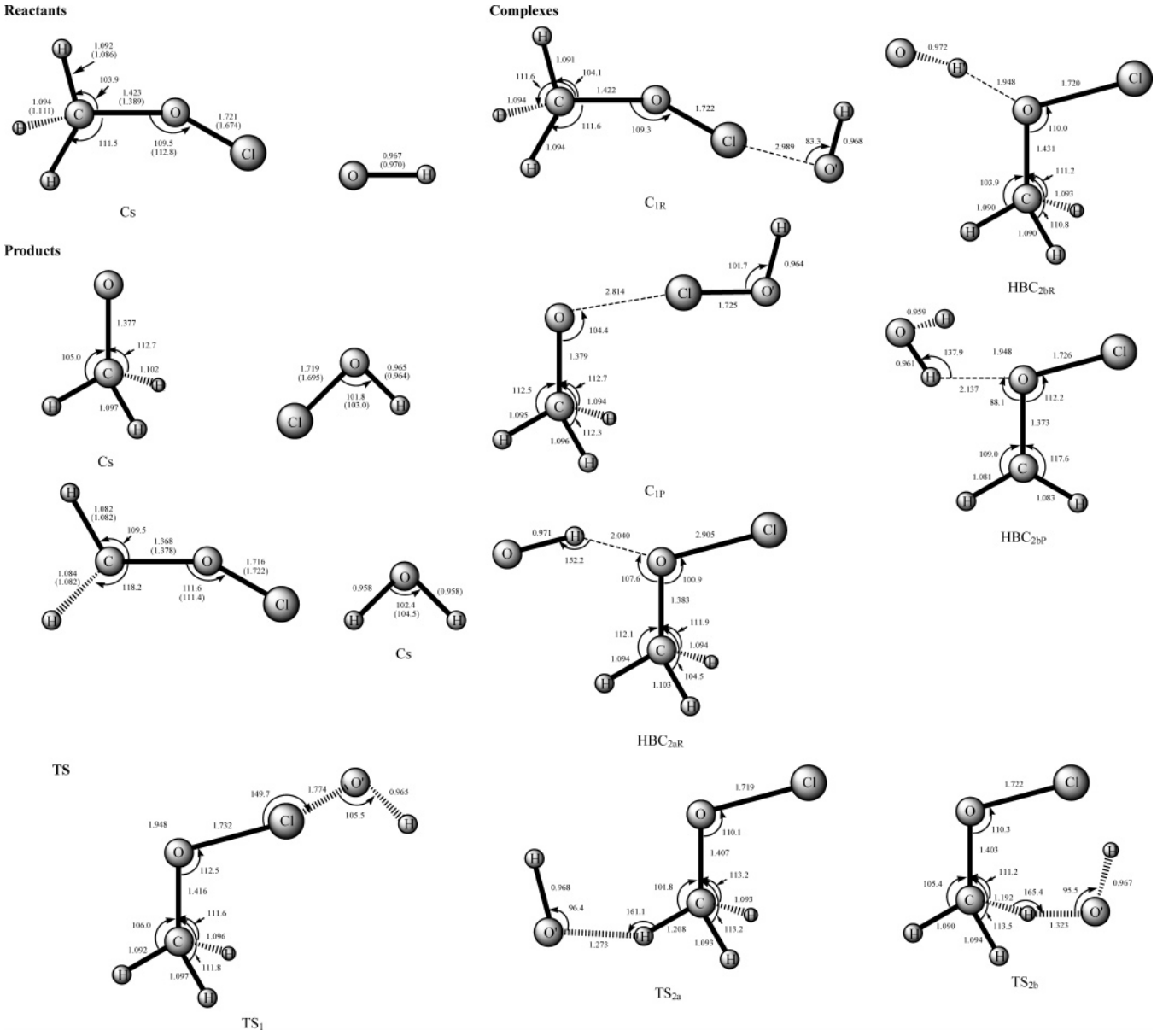

Figure 1. Optimized geometries of reactants, products, complexes, and transition states at the MP2/6-311G(d,p) level of the reaction CH_3OCl + OH. The numbers in parentheses are the experimental values.[26−29] Bond lengths are in angstroms, and angles are in degrees.

By means of the POLYRATE 8.4.1 program,[18] the theoretical rate constants and activation energies are calculated by using canonical variational transition state theory (CVT)[19−21] with the small-curvature tunneling correction (SCT)[22,23] method approximation. All vibrational modes other than the lowest-vibrational one are treated harmonically, and for the lowest-frequency modes the partition functions are calculated by the hindered rotor approximation of Truhlar and Chuang.[24,25] In the calculation of the electronic partition functions, the two electronic states for OH radicals, with a 140 cm^{-1} splitting in the $^2\Pi$ ground state, are included. The curvature components are calculated using a quadratic fit to obtain the derivative of the gradient with respect to the reaction coordinate.

Result and Discussion

(1) Stationary Points. For Cl-abstraction reaction R1, only one pathway is found. Because CH_3OCl has C_s symmetry, the two out-of-plane hydrogen atoms are equivalent, which are different from the in-plane hydrogen; as a result, two possible pathways, in-plane H-abstraction (R2a) and out-of-plane H-abstraction (R2b), are found. Thus, three transition states, one for Cl-abstraction (TS_1) and two for H-abstraction (TS_{2a} and TS_{2b}), are located at the MP2/6-311G(d,p) level. Two complexes, one at the reactant side and one at the product side, are located for R1 and R2b, respectively, and for in-plane H-abstraction reaction R2a, only one hydrogen-bonded complex is at the entrance of this channel. The optimized geometric parameters of the reactants (CH_3OCl and OH), complexes, transition states (TSs), and products (CH_3O, HOCl, CH_2OCl, and H_2O) at the MP2/6-311G(d,p) level are shown in Figure 1 along with the available experimental values.[26−29] As shown in Figure 1, when a comparison is possible, the optimized parameters of the reactants (CH_3OCl and OH), the products (CH_3O, HOCl, CH_2OCl, and H_2O), and the complexes obtained at the MP2/6-311G(d,p) level show good agreement with the experiments, and the bond lengths of the reactants and products agree with the experiment data with the largest discrepancy of 0.05 Å. In R1, the distances of the O′−Cl bond in complex C_{1R} and the O−Cl bond in complex C_{1P} are 2.989 and 2.814 Å, respectively, and the other bond lengths in these two

TABLE 1: Calculated and Experimental Frequencies (cm^{-1}) of the Equilibrium and Transition-State Structures for the Reaction at the MP2/6-311G(d,p) Level

	MP2/6-311G(d,p)	exptl
CH_3OCl	3191, 3154, 3067, 1532, 1488, 1488, 1217, 1199, 1064, 673, 374, 283	3144, 3117, 3040, 1516, 1479, 1467, 1201, 1180, 1046, 692, 373, 254[a]
OH	3853	3735[b]
CH_3O	3128, 3094, 3014, 1552, 1433, 1429, 1142, 990, 822	3609, 2946, 2862, 1471, 1371, 1355, 1065, 926, 776[c]
HOCl	3845, 1223, 723	3609, 1239, 724[b]
CH_2OCl	3332, 3176, 1487, 1205, 1163, 740, 678, 396,308	3388, 3231, 1595, 1209, 1162, 784, 691, 398, 287[d]
H_2O	4011, 3904, 1668	3756, 3657, 1595[b]
C_{1R}	3841, 3191, 3151, 3065, 1532, 1489, 1217, 1199, 1067, 674, 381, 281, 250, 106, 99, 44, 27	
C_{1P}	3853, 3143, 3102, 3017, 1548, 1438, 1215, 1139, 1023, 945, 715, 147, 118, 100, 73, 54, 47	
HBC_{2aR}	3775, 3168, 3114, 3017, 1543, 1434, 1127, 1047, 972, 531, 371, 191, 130, 91, 69, 38, 20	
HBC_{2bR}	3756, 3209, 3178, 3083, 1529, 1491, 1488, 1219, 1048, 681, 575, 447, 277, 170, 91, 36	
HBC_{2bP}	3984, 3883, 3348, 3184, 1685, 1477, 1204, 1149, 741, 703, 466, 399, 190, 164, 145, 92, 44	
TS_1	3849, 3177, 3125, 3046, 1523, 1497, 1484, 1205, 1193, 1072, 1042, 686, 447, 372, 314, 196, 153, 297i	
TS_{2a}	3834, 3194, 3100, 1571, 1520, 1255, 1247, 1156, 1134, 904, 849, 699, 356, 317, 164, 110, 62, 2027i	
TS_{2b}	3842, 3217, 3106, 1546, 1477, 1329, 1243, 1188, 1096, 877, 773, 673, 382, 356, 150, 133, 76, 1859i	

[a] From ref 30. [b] From ref 27. [c] From ref 31. [d] From ref 32.

TABLE 2: Relative Enthalpies ($\Delta H_{298}°$) and Potential Barriers (ΔE) (kcal mol^{-1}) with ZPE Correction at the a-QCISD(T)//MP2, G3//MP2, and G3(MP2)//MP2 Levels

	levels		MP2/6-311G(d,p)	a-QCISD(T)/6-311++G(3df,2pd)	G3	G3(MP2)	exptl
$CH_3OCl + OH \rightarrow$		TS_1	20.5	2.85	3.15	4.04	
$CH_3O + HOCl$	ΔE	C_{1R}	−2.13	−1.86	−1.35	−0.83	
		C_{1P}	−6.66	−8.63	−8.82	−8.24	
			−4.23	−6.16	−6.42	−5.93	
	$\Delta H_{298}°$						-7.67 ± 2.5,[a] -8.89[b]
$CH_3OCl + OH \rightarrow$		TS_{2a}	6.33	3.82	4.84	5.02	
$CH_2OCl + H_2O$		TS_{2b}	7.32	1.46	2.62	3.83	
	ΔE	HBC_{2aR}	−3.92	−2.86	−2.95	−2.63	
		HBC_{2bR}	−4.55	−2.63	−2.65	−1.91	
		HBC_{2bP}	−21.8	−20.8	−20.2	−19.6	
			−17.6	−19.0	−18.5	−18.1	
	$\Delta H_{298}°$						-19.4 ± 2.2,[c] -22.7[b]

[a] From refs 27 and 33. [b] From ref 5. [c] From refs 27, 33, and 34.

complexes are very close to those of the corresponding reactants and products. Similarly, in the hydrogen-bonded complexes HBC_{2aR}, HBC_{2bR}, and HBC_{2bP} structures, O−H bond distances are 2.04, 1.948, and 2.137 Å, less than the sum of van der Waals radii, and the other bond lengths are also close to those of the reactants and products. For the transition state, TS_1, the O−Cl bond, which will be broken, is elongated by 1% as compared to the O−Cl length in the isolated CH_3OCl, and the forming bond O′−Cl is 3% longer than the equilibrium bond length of HOCl. The elongation of the forming bond (O′−Cl) is almost equal to that of the breaking bond (O−Cl), which indicates reaction R1 proceeds via a near symmetrical barrier. The calculations predict 33% (in TS_{2a}) and 38% (in TS_{2b}) stretching of the O−H bond as compared to the O−H length in the isolated H_2O, and the calculations also predict 11% and 9% stretching of the C−H bond as compared to the C−H length in the isolated CH_3OCl. These structural parameters indicate that TS_{2a} and TS_{2b} are all reactant-like and R2 proceeds via an early transition state.

Table 1 lists the harmonic vibrational frequencies of all of the stationary points of the reaction $CH_3OCl + OH$ at the MP2/6-311G(d,p) level along with the available experimental data.[27,30−32] The equilibrium (including the reactants, products, and complexes) possesses all real frequencies, and it shows that most of the calculated frequencies agree generally well with the available experimental values. The transition states are identified with one and only one imaginary frequency, which takes the values of 297i, 2027i, and 1859i for TS_1, TS_{2a}, and TS_{2b}, respectively.

The reaction enthalpies ($\Delta H_{298}°$) and the relative energies (ΔE) with zero-point energy (ZPE) corrections of the complexes and TSs calculated at various levels are listed in Table 2. It is shown that at the a-QCISD(t)/6-311++G(3df,2pd)//MP2/6-311G(d,p) level, the complexes located at the entrance of the three reaction channels are 1.86, 2.86, and 2.63 kcal/mol more stable than the reactants $CH_3OCl + OH$, and the energies of complexes C_{1P} and HBC_{2bP} are about 2.47 and 1.8 kcal/mol lower than the products $CH_3O + HOCl$ and $CH_2OCl + H_2O$, respectively. The calculations at the other two high levels predict similar results. At the MP2/6-311G(d,p) level, the reaction enthalpy takes the value of −4.23 kcal/mol for reaction R1, while the corresponding values are −6.16, −6.42, and −5.93 kcal/mol at three high levels, a-QCISD(T)//MP2, G3//MP2, and G3(MP2)//MP2, respectively. The results show good agreement with the experimental values of -7.67 ± 2.5 kcal/mol (CH_3-

TABLE 3: Rate Constants (cm^3 $molecule^{-1}$ s^{-1}) for the Reaction $CH_3OCl + OH$ in the Temperature Range 220−2000 K[a]

T (K)	k_1	k_{2a}	k_{2b}	k_2	k	exptl[b]
220	3.68×10^{-14}	5.72×10^{-15}	1.91×10^{-13}	1.97×10^{-13}	2.34×10^{-13}	
235	3.78×10^{-14}	6.38×10^{-15}	2.22×10^{-13}	2.28×10^{-13}	2.66×10^{-13}	
250	3.90×10^{-14}	7.14×10^{-15}	2.56×10^{-13}	2.63×10^{-13}	3.02×10^{-13}	$(5.74 \pm 0.38) \times 10^{-13}$
260	3.99×10^{-14}	7.72×10^{-15}	2.81×10^{-13}	2.89×10^{-13}	3.29×10^{-13}	$(6.15 \pm 0.35) \times 10^{-13}$
267	4.06×10^{-14}	8.15×10^{-15}	2.99×10^{-13}	3.07×10^{-13}	3.48×10^{-13}	$(5.85 \pm 0.46) \times 10^{-13}$
268	4.07×10^{-14}	8.21×10^{-15}	3.02×10^{-13}	3.10×10^{-13}	3.51×10^{-13}	$(5.57 \pm 0.54) \times 10^{-13}$
283	4.24×10^{-14}	9.23×10^{-15}	$3.44 \times 10_{-13}$	3.53×10^{-13}	3.96×10^{-13}	$(6.60 \pm 0.38) \times 10^{-13}$
294	4.37×10^{-14}	1.01×10^{-14}	3.77×10^{-13}	3.87×10^{-13}	4.31×10^{-13}	$(7.13 \pm 0.60) \times 10^{-13}$
298	4.42×10^{-14}	1.04×10^{-14}	3.90×10^{-13}	4.00×10^{-13}	4.45×10^{-13}	
322	4.74×10^{-14}	1.25×10^{-14}	4.70×10^{-13}	4.83×10^{-13}	5.30×10^{-13}	$(7.37 \pm 0.42) \times 10^{-13}$
341	5.02×10^{-14}	1.45×10^{-14}	5.42×10^{-13}	5.57×10^{-13}	6.07×10^{-13}	$(8.37 \pm 0.45) \times 10^{-13}$
400	6.06×10^{-14}	2.27×10^{-14}	8.00×10^{-13}	8.23×10^{-13}	8.83×10^{-13}	
500	8.37×10^{-14}	4.51×10^{-14}	1.38×10^{-12}	1.43×10^{-12}	1.51×10^{-12}	
800	1.98×10^{-13}	2.21×10^{-13}	4.39×10^{-12}	4.61×10^{-12}	4.81 × 10-12	
1000	3.17×10^{-13}	4.81×10^{-13}	7.84×10^{-12}	8.32×10^{-12}	8.64×10^{-12}	
1200	4.73×10^{-13}	9.03×10^{-13}	1.29×10^{-11}	1.38×10^{-11}	1.43×10^{-11}	
1400	6.69×10^{-13}	1.53×10^{-12}	1.96×10^{-11}	2.11×10^{-11}	2.18×10^{-11}	
1700	1.04×10^{-12}	2.92×10^{-12}	3.31×10^{-11}	3.60×10^{-11}	3.71×10^{-11}	
2000	1.51×10^{-12}	4.94×10^{-12}	5.10×10^{-11}	5.59×10^{-11}	5.75×10^{-11}	

[a] k_1, k_{2a}, k_{2b}, and k_2 ($k_2 = k_{2a} + k_{2b}$) represent the canonical variational transition-state theory (CVT) with the small curvature tunneling (SCT) rate constants of reactions R1 and R2, respectively, and k represents the total rate constant of reaction calculated from the sum of the three CVT/SCT rate constants at the a-QCISD(T)/6-311++G(3df,2pd)//MP2/6-311G(d,p) level. [b] From ref 5.

OCl, −13.2 ± 2.3 kcal/mol,[33] OH, 9.33 kcal/mol,[27] CH_3O, 4.07 kcal/mol,[27] and HOCl, −17.82 kcal/mol[27]) and −8.89 kcal/mol.[5] For H-abstraction R2, all of the three high-level $\Delta H_{298}°$ values, which are −19.0, −18.5, and −18.1 kcal/mol, respectively, correlate well with the experimental ones, −19.4 ± 2.2 kcal/mol (CH_2OCl, 32.0 ± 3.5 kcal/mol[34] and H_2O, −57.58 kcal/mol[27]) and −22.7 kcal/mol.[5]

With respect to the potential barriers (ΔE) given in Table 2, we note that although the chlorine-abstraction channel (R1) involves a higher potential energy barrier (ca. 20 kcal/mol) at the MP2/6-311G(d,p) level, TS_1 lies higher than the reactants by about 2.85, 3.15, and 4.04 kcal/mol at the a-QCISD(T)//MP2, G3//MP2, and G3(MP2)//MP2 levels, respectively, and it is about 4.71, 4.5, and 4.87 kcal/mol higher than the complex C_{1R}. As for TS_{2a} and TS_{2b}, the ΔE results are 3.82, 4.84, and 5.02 kcal/mol for R2a, and 1.46, 2.62, and 3.83 kcal/mol for R2b at the three different high levels, respectively. A schematic potential energy surface of the reaction obtained at the a-QCISD-(T)//MP2 level is plotted in Figure 2. Seen from Figure 2, the barrier height of Cl-abstraction channel, TS_1 (2.85 kcal/mol), is about 1.4 kcal/mol higher than that of the out-of-plane H-abstraction channel, TS_{2b} (1.46 kcal/mol), and about 1 kcal/mol lower than that of the in-plane H-abstraction channel, TS_{2a} (3.82 kcal/mol). It shows that the order of kinetic stability of these three transition states is $TS_{2b} > TS_1 > TS_{2a}$. Also, the reaction enthalpies of R1 and R2 are −6.16 and −19.00 kcal/mol, respectively, which indicates the products of H-abstraction reaction are far more thermodynamically stable than those of the Cl-abstraction reaction. Thus, it might be expected that abstraction will occur mainly from out-of-plane hydrogen and plays a more important role than the other two abstraction pathways in the reaction $CH_3OCl + OH$. This view is further testified in the following rate constants study.

(2) Dynamic Calculations. The $CH_3OCl + OH$ reaction involves three possible reaction pathways: abstraction from chlorine atom, in-plane, and out-of-plane hydrogen atoms, respectively. The total rate constant is obtained from the sum of the individual rate constants associated with the three reaction channels. The PES information for each reaction channel, which is obtained at the a-QCISD(T)/6-311++G(3df,2pd)//MP2/6-311G(d,p) level, is put into the POLYRATE 8.4.1 program to produce the VTST rate constants in a wide temperature range

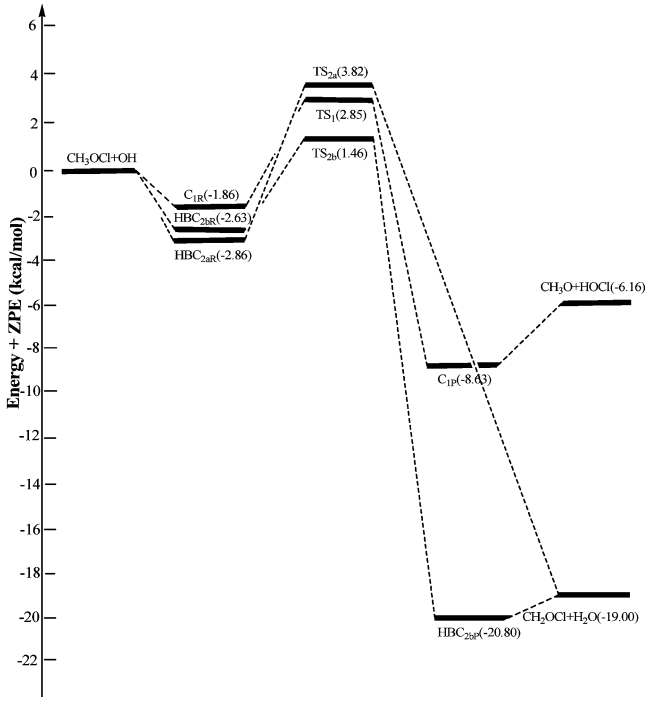

Figure 2. Schematic potential energy surface for the reaction $CH_3OCl + OH$. Relative energies (in kcal/mol) are calculated at the a-QCISD(T)/6-311++G(3df,2pd)//MP2/6-311G(d,p) + ZPE level (the values in parentheses).

from 220 to 2000 K. The theoretical total rate constants $k = k_1 + k_2$ ($k_2 = k_{2a} + k_{2b}$) and the available experimental values are described in Table 3 and Figure 3, and the temperature dependence of the k_1/k and k_2/k branching ratios is exhibited in Figure 4. From Figure 3, we can find that the activation energy is 1.3 kcal/mol in 250−341 K, and the calculated rate constants are in good agreement with the available experimental values,[5] with the deviation factor of 1.4−1.9 in the temperature range 250−341 K. The theoretical branching ratios of k_2/k are about 0.84−0.97 in the temperature region 220−2000 K, which suggests that the reaction of CH_3OCl with OH proceeds predominantly via H-abstraction over the whole temperature range, and the contribution of chlorine abstraction to the total rate constant is considerably less. This result supports the

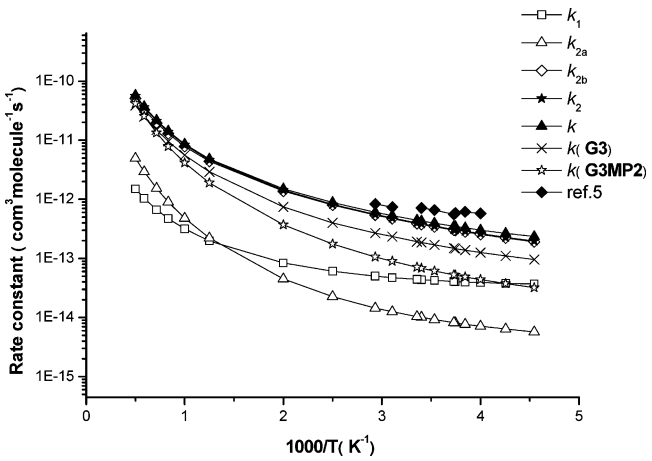

Figure 3. Calculated rate constants, k_1, for the reaction $CH_3OCl + OH \rightarrow CH_3O + HOCl$, k_2 ($k_2 = k_{2a} + k_{2b}$) for the reaction $CH_3OCl + OH \rightarrow CH_2OCl + H_2O$, and total rate constant k ($k = k_1 + k_2$) along with the experimental values as a function of 1000/T at a-QCISD(T)/6-311++G(3df,2pd)//MP2/6-311G(d,p). k(G3) and k(G3(MP2)) represent the total rate constants at the G3//MP2/6-311G(d,p) and G3(MP2)//MP2/6-311G(d,p) levels.

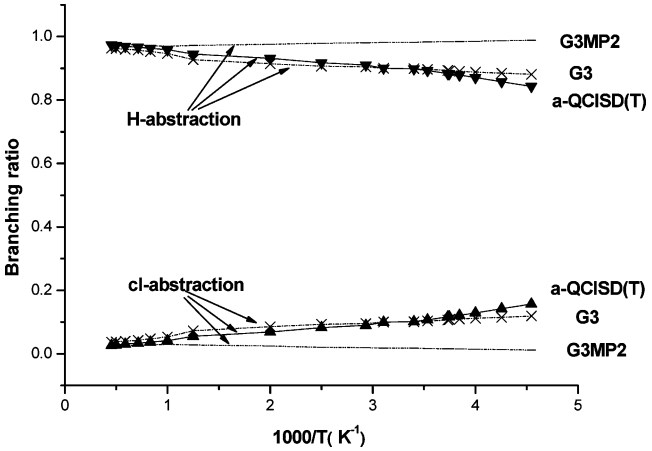

Figure 4. Calculated branching ratio for the $CH_3OCl + OH$ reaction as a function of 1000/T at three high levels, respectively.

conclusion proposed by Crowley et al. who assumed 100% branching to CH_2OCl,[5] in opposition to the result obtained by Kukui et al.,[6] in which CH_3O was identified as the major product (ca. 80% branching). Our calculated two-parameter Arrhenius expression for the reaction $CH_3OCl + OH$ in the temperature range 250−341 K, $k = 4.01 \times 10^{-12} \exp(-651.8/T)$ cm^3 molecule^{-1} s^{-1}, is consistent with the experimental Arrhenius expression reported by Crowley et al.,[5] $k = (2.4 \pm 0.8) \times 10^{-12} \exp(-(360\pm100)/T)$ cm^3 molecule^{-1} s^{-1}. To further investigate the temperature dependence of the rate constants and branching ratios for the title reaction, the dynamic calculations are performed at the other two levels G3//MP2 and G3(MP2)//MP2, respectively, which are exhibited in the same figures as those at the a-QCISD(T)//MP2 level. It can be seen that the G3//MP2 and G3(MP2)//MP2 results slightly underestimate the experimental values in 250−341 K, but the calculated results at these three levels do not differ greatly. Also, the similarities in the branching ratios at three high levels imply that for the $CH_3OCl + OH$ reaction, abstraction by OH occurs almost exclusively to yield product $CH_2OCl + H_2O$, while the chlorine abstraction channel may be negligible.

The rate constants exhibit strong non-Arrhenius behavior in the temperature range of 220−2000 K. Due to the lack of the experimental data in other temperature ranges, the three-parameter fits based on the predicted a-QCISD(T)//MP2 rate constants for the total reaction give the expressions as follows (in units of cm^3 molecule^{-1} s^{-1}):

$$k_1 = 1.87 \times 10^{-19} T^{2.67} \exp(534.6/T)$$

$$k_{2a} = 6.12 \times 10^{-23} T^{3.89} \exp(415.1/T)$$

$$k_{2b} = 5.06 \times 10^{-18} T^{2.72} \exp(108.2/T)$$

$$k_2 = 3.45 \times 10^{-18} T^{2.78} \exp(126.0/T)$$

$$k = 2.38 \times 10^{-18} T^{2.83} \exp(184.7/T)$$

Conclusions

In this paper, the multichannel reaction $CH_3OCl + OH \rightarrow CH_3O + HOCl$ (R1) and $CH_2OCl + H_2O$ (R2) has been studied by an ab initio direct dynamics method. The potential energy surface (PES) information is obtained at the MP2/6-311G(d,p) level, and higher-level energies at the stationary points and extra points along the reaction path are calculated at the a-QCISD-(T)/6-311++G(3df,2pd), G3, and G3(MP2) levels. The theoretical rate constants in the temperature range 220−2000 K are calculated by canonical variational transition state theory (CVT) with the small-curvature tunneling correction (SCT). The total rate constants obtained at the a-QCISD(T)/6-311++G(3df,2pd)//MP2/6-311G(d,p) level are in better agreement with the experimental values in the measured temperature range. The three higher-level dynamic calculations show that the reaction proceeds dominantly via hydrogen abstraction leading to the formation of $CH_2OCl + H_2O$ over the whole temperature range.

Acknowledgment. We thank Professor Donald G. Truhlar for providing the POLYRATE 8.4.1 program. This work is supported by the National Natural Science Foundation of China (20333050, 20303007), the Doctor Foundation by the Ministry of Education, the Foundation for University Key Teacher by the Ministry of Education, Key Subject of Science and Technology by the Ministry of Education of China, and the Innovation Foundation by Jilin University.

References and Notes

(1) Abbatt, J. P. D.; Molina, M. J. *Geophys. Res. Lett.* **1992**, *19*, 461.
(2) Forman, J. C.; Gardiner, B. G.; Shanklin, J. D. *Nature* **1985**, *315*, 207.
(3) Solomon, S. *Nature* **1990**, *347*, 347.
(4) Helleis, F.; Crowley, J. N.; Moortgat, G. K. *J. Phys. Chem.* **1993**, *97*, 11464.
(5) Crowley, J. N.; Campuzano-Jost, P.; Moortgat, G. K. *J. Phys. Chem.* **1996**, *100*, 3601.
(6) Kukui, A.; Benter, Th.; Schindler, R. N. Data presented at the 2nd Euroconfence: "6th sensing the atmosphere"; Marbella, Spain, 1996.
(7) Truhlar, D. G. In *The Reaction Path in Chemistry: Current Approaches and Perspectives*; Heidrich, D., Ed.; Kluwer: Dordrecht, The Netherlands, 1995; p 229.
(8) Truhlar, D. G.; Garrent, B. C.; Klippenstein, S. J. *J. Phys. Chem.* **1996**, *100*, 12771.
(9) Hu, W. P.; Truhlar, D. G. *J. Am. Chem. Soc.* **1996**, *118*, 860.
(10) Truhlar, D. G.; Garrett, B. C. *Acc. Chem. Res.* **1980**, *13*, 440.
(11) Truhlar, D. G.; Isaacson, A. D.; Garrett, B. C. In *The Theory of Chemical Reaction Dynamics*; Baer, M., Ed.; CRC Press: Boca Raton, FL, 1985; p 65.
(12) Truhlar, D. G.; Garrett, B. C. *Annu. Rev. Phys. Chem.* **1984**, *35*, 159.
(13) Frisch, M. J.; Truck, G. W.; Schlegel, H. B.; Scuseria, G. E.; Robb, M. A.; Cheeseman, J. R.; Zakrzewski, V. G.; Montgomery, J. A., Jr.; Stratmann, R. E.; Burant, J. C.; Dapprich, S.; Millam, J. M.; Daniels, A. D.; Kudin, K. N.; Strain, M. C.; Farkas, O.; Tomasi, J.; Barone, V.; Cossi, M.; Cammi, R.; Mennucci, B.; Pomelli, C.; Adamo, C.; Clifford, S.; Ochterski, J.; Petersson, G. A.; Ayala, P. Y.; Cui, Q.; Morokuma, K.; Malick,

D. K.; Rabuck, A. D.; Raghavachari, K.; Foresman, J. B.; Cioslowski, J.; Ortiz, J. V.; Boboul, A. G.; Stefnov, B. B.; Liu, G.; Liaschenko, A.; Piskorz, P.; Komaromi, L.; Gomperts, R.; Martin, R. L.; Fox, D. J.; Keith, T.; Al-Laham, M. A.; Peng, C. Y.; Nanayakkara, A.; Gonzalez, C.; Challacombe, M.; Gill, P. M. W.; Johnson, B.; Chem, W.; Wong, M. W.; Andres, J. L.; Head-Gordon, M.; Replogle, E. S.; Pople, J. A. *Gaussian 98*, revision X; Gaussian, Inc.: Pittsburgh, PA, 1998.

(14) Thiesemann, H.; Clifford, E. P.; Taatjes, C. A.; Stephen, J.; Klippenstein, S. J. *J. Phys. Chem. A* **2001**, *105*, 5393.

(15) Curtiss, L. A.; Raghavachari, K.; Redforn, P. C.; Rassolov, V.; Pople, J. A. *J. Chem. Phys.* **1998**, *109*, 7764.

(16) Curtiss, L. A.; Redfern, P. C. *J. Chem. Phys.* **1999**, *110*, 10.

(17) Chuang, Y. Y.; Corchado, J. C.; Truhlar, D. G. *J. Phys. Chem.* **1999**, *103*, 1140.

(18) Chuang, Y. Y.; Corchado, J. C.; Fast, P. L.; Villa, J.; Hu, W. P.; Liu, Y. P.; Lynch, G. C.; Jackels, C. F.; Nguyen, K. A.; Gu, M. Z.; Rossi, I.; Coitino, E. L.; Clayton, S.; Melissas, V. S.; Lynch, B. J.; Steckler, R.; Garrett, B. C.; Isaacson, A. D.; Truhlar, D. G. *Polyrate version 8.4.1*; University of Minnnesota: Minneapolis, 2000.

(19) Garrett, B. C.; Truhlar, D. G. *J. Chem. Phys.* **1979**, *70*, 1593.

(20) Garrett, B. C.; Truhlar, D. G. *J. Am. Chem. Soc.* **1979**, *101*, 4534.

(21) Garrett, B. C.; Truhlar, D. G.; Grev, R. S.; Magnuson, A. W. *J. Phys. Chem.* **1980**, *84*, 1730.

(22) Lu, D. H.; Truong, T. N.; Melissas, V. S.; Lynch, G. C.; Liu, Y. P.; Grarrett, B. C.; Steckler, R.; Issacson, A. D.; Rai, S. N.; Hancock, G. C.; Lauderdale, J. G.; Joseph, T.; Truhlar, D. G. *Comput. Phys. Commun.* **1992**, *71*, 235.

(23) Liu, Y. P.; Lynch, G. C.; Truong, T. N.; Lu, D. H.; Truhlar, D. G.; Garrett, B. C. *J. Am. Chem. Soc.* **1993**, *115*, 2408.

(24) Truhlar, D. G. *J. Comput. Chem.* **1991**, *12*, 266.

(25) Chuang, Y. Y.; Truhlar, D. G. *J. Chem. Phys.* **2000**, *112*, 1221.

(26) Rigden, J. S.; Butchers, S. S. *J. Chem. Phys.* **1964**, *40*, 2109.

(27) Chase, M. W., Jr. NIST-JANAF Themochemical Tables, 4th ed. *J. Phys. Chem. Ref. Data* **1998**, Monograph 9, 1−1951.

(28) Kuchitsu, K. *Structure of Free Polyatomic Molecules: Basic Data*; Springer: Berlin, 1998; Vol. 1, p 35.

(29) Messer, B. M.; Elrod, M. J. *Chem. Phys. Lett.* **1999**, *301*, 10.

(30) Francisco, J. S. *Int. J. Quantum Chem.* **1999**, *73*, 29.

(31) He, T. J.; Chen, D. M.; Liu, F. C.; Sheng, L. S. *Chem. Phys. Lett.* **2000**, *332*, 545.

(32) Melius, C. Wrb ssite: (a) http://z.casandia.gov/∼melius/; July, 2000. http://www.cstl.nist.gov/div836/ckmech/SpeciedData.html; July, 2000.

(33) Espinosa-Garcia, J. *Chem. Phys.* **1999**, *315*, 239.

(34) Espinosa-Garcia, J. *Chem. Phys. Lett.* **2000**, *316*, 563.